[Supporting Information]

Synthesis, structure and stability of three V-substituted polyoxoniobate clusters based on $[TeNb_9O_{33}]^{17-}$ units

Zongfei Yang, Jingjing Shang, Yuanyuan Yang, Pengtao Ma, Jingyang Niu,* and Jingping Wang*

Henan Key Laboratory of Polyoxometalate Chemistry, Institute of Molecular and Crystal Engineering, College of Chemistry and Chemical Engineering, Henan University, Kaifeng 475004, Henan (P.R. China)
E-mail: jyniu@henu.edu.cn, jpwang@henu.edu.cn, Fax: (+86)371-23886876

CONTENTS

Section 1 Experimental Section

1. X-ray Crystallography

The suitable crystals of **1-3** were selected and the structural measurements were performed at 149.98 K on a Bruker Apex-II CCD diffractometer using graphite-monochromated Mo Kα radiation (λ = 0.71073 Å). After data collection, Dates reduction, including a correction for routine Lorentz and polarization, was performed by an applied multiscan absorption correction SADABS program.[S1] The crystal structures were solved by the direct method and refined by full matrix least-squares on all F^2 data using the SHELX program suite.[S2-3] In the final refinement, the Nb, Te, V and Cu atoms of **1-3** were refined anisotropically. Moreover, the partial lattice water molecules were located by Fourier map; the remaining lattice water molecules were determined by CHN element analysis and TGA results. CCDC numbers are **1952796**, **2003142** and **2003141** for compounds **1-3**, respectively.

Section 2 Supplementary Structural Figures and Tables

The bond-valence-sum (BVS) calculations of **1a** confirm that the oxidation states of all tellurium, copper, vanadium and niobium centers are +4, +2, +5 and +5, respectively (Table S4).[S4] The BVS calculations give values of 0.19 and 0.29 for O1W and O2W, respectively, which indicate that the oxygen atoms can be bisprotonated (Table S1). Likewise, BVS calculations of tellurium, oxygen, copper, niobium and vanadium centers in **2a** and **3a** are also performed in the ESI (Table S2, S3, S5, S6). Further, the oxidation states of Te, Cu and V centers in compounds **1-3** were also evidenced through X-ray photoelectron spectra (XPS) measurements (Figure S1-S3).

Table S1 Bond valence sum calculations of the oxygen atoms of compound **1**.

Atom label	Bond valence Sum	Atom label	Bond valence Sum	Atom label	Bond valence Sum	Atom label	Bond valence Sum
O1	2.13	O12	1.78	O23	1.78	O34	1.62
O2	1.83	O13	1.60	O24	1.69	O35	1.52
O3	1.65	O14	1.79	O25	1.68	O36	1.50
O4	1.91	O15	1.68	O26	1.74	O37	1.85
O5	1.48	O16	1.07	O27	1.81	O1W	0.19
O6	1.82	O17	1.13	O28	1.54	O2W	0.29
O7	1.53	O18	1.68	O29	1.48	O11	1.89
O8	1.69	O19	2.15	O30	1.46	O22	1.88
O9	1.85	O20	2.13	O31	0.90	O33	1.92
O10	1.50	O21	2.08	O32	1.73		

Table S2 Bond valence sum calculations of the oxygen atoms of compound **2**.

Atom label	Bond valence Sum	Atom label	Bond valence Sum	Atom label	Bond valence Sum	Atom label	Bond valence Sum
O1	1.48	O12	1.43	O23	1.88	O34	1.82
O2	1.44	O13	1.40	O24	1.67	O35	2.12
O3	1.46	O14	1.98	O25	1.44	O36	1.72
O4	1.47	O15	1.67	O26	1.84	O38	1.89
O5	1.46	O16	1.91	O27	1.67	O39	1.84
O6	1.53	O17	1.50	O28	1.92	O40	1.86
O7	1.46	O18	2.06	O29	1.86	O11	1.48
O8	1.59	O19	2.09	O30	1.67	O22	2.08
O9	1.45	O20	2.00	O31	2.19	O33	1.83
O10	1.38	O21	1.74	O32	1.78		

Table S3 Bond valence sum calculations of the oxygen atoms of compound **3**.

Atom label	Bond valence Sum	Atom label	Bond valence Sum	Atom label	Bond valence Sum	Atom label	Bond valence Sum
O1	1.49	O12	1.70	O23	1.56	O34	1.25
O2	1.73	O13	1.53	O24	1.80	O35	2.01
O3	1.71	O14	1.39	O25	1.47	O36	1.48
O4	1.84	O15	2.06	O26	2.04	O37	1.48
O5	1.86	O16	1.50	O27	1.80	O38	1.94
O6	1.42	O17	1.84	O28	1.46	O39	1.60
O7	1.71	O18	1.51	O29	1.52	O11	1.70
O8	1.86	O19	2.07	O30	1.93	O22	1.73.
O9	1.67	O20	1.82	O31	2.01	O33	1.46
O10	1.41	O21	1.46	O32	1.49		

Table S4 Bond valence sum calculations of the Nb, Te, V and Cu atoms of compound **1**.

Atom Code	Bond Valence	Valence state	Atom Code	Bond Valence	Valence state	Atom Code	Bond Valence	Valence state
Nb1	5.04	+5	Nb8	5.05	+5	Cu3	2.13	+2
Nb2	4.92	+5	Nb9	4.98	+5	Cu4	2.15	+2
Nb3	4.99	+5	Te1	3.94	+4	Nb7	5.02	+5
Nb4	4.91	+5	V1	5.20	+5	Cu2	2.22	+2
Nb5	5.03	+5	V2	5.10	+5			
Nb6	4.94	+5	Cu1	2.17	+2			

Table S5 Bond valence sum calculations of the Nb, Te, V and Cu atoms of compound **2**.

Atom Code	Bond Valence	Valence state	Atom Code	Bond Valence	Valence state	Atom Code	Bond Valence	Valence state
V1	5.27	+5	Cu3	1.66	+2	Nb6	5.03	+5
V2	5.10	+5	Nb1	4.81	+5	Nb7	4.84	+5
V3	5.07	+5	Nb2	4.92	+5	Nb8	5.07	+5
Te1	4.10	+4	Nb3	4.89	+5	Nb9	4.97	+5
Cu1	1.69	+2	Nb4	4.92	+5			
Cu2	1.77	+2	Nb5	4.85	+5			

Table S6 Bond valence sum calculations of the Nb, Te, V and Cu atoms of compound **3**.

Atom Code	Bond Valence	Valence state	Atom Code	Bond Valence	Valence state	Atom Code	Bond Valence	Valence state
V1	5.10	+5	Cu3	1.70	+2	Nb6	4.96	+5
V2	5.11	+5	Nb1	4.95	+5	Nb7	4.93	+5
V3	5.03	+5	Nb2	4.94	+5	Nb8	4.92	+5
Te1	3.95	+4	Nb3	4.95	+5	Nb9	4.96	+5
Cu1	1.70	+2	Nb4	4.94	+5			
Cu2	1.75	+2	Nb5	4.95	+5			

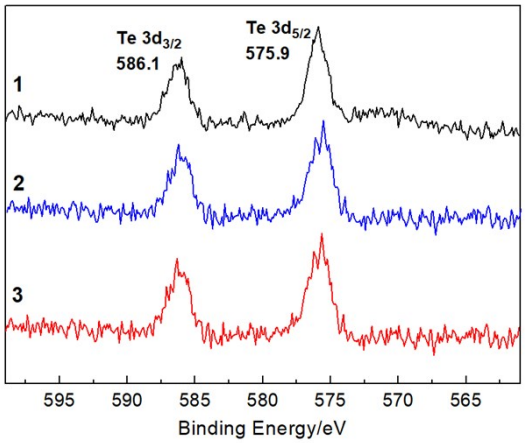

Figure S1 XPS spectrum of Te 3d (Te^{IV} $3d_{3/2}$, 586.1; Te^{IV} $3d_{5/2}$, 575.9) in compounds **1-3**.[S5]

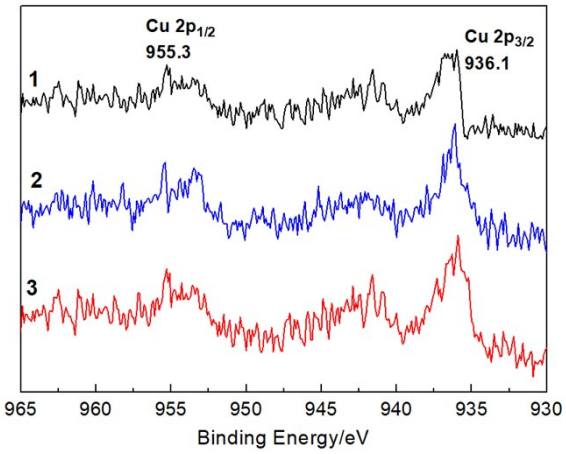

Figure S2 XPS spectrum of Cu 2p (Cu^{II} $2P_{1/2}$, 955.3; Cu^{II} $2P_{3/2}$, 936.1) in compounds **1-3**.[S6]

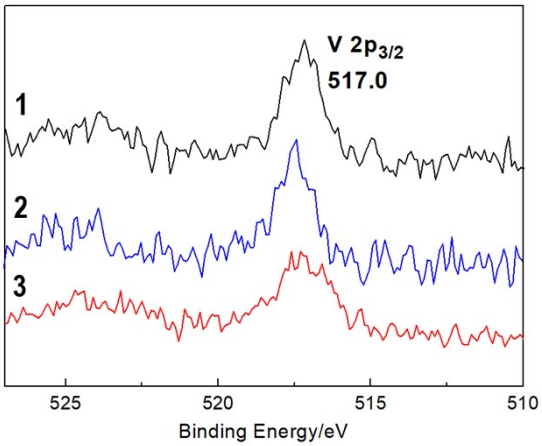

Figure S3 XPS spectrum of V 2p (V^V $2P_{3/2}$, 517.0) in compounds **1-3**.[S7]

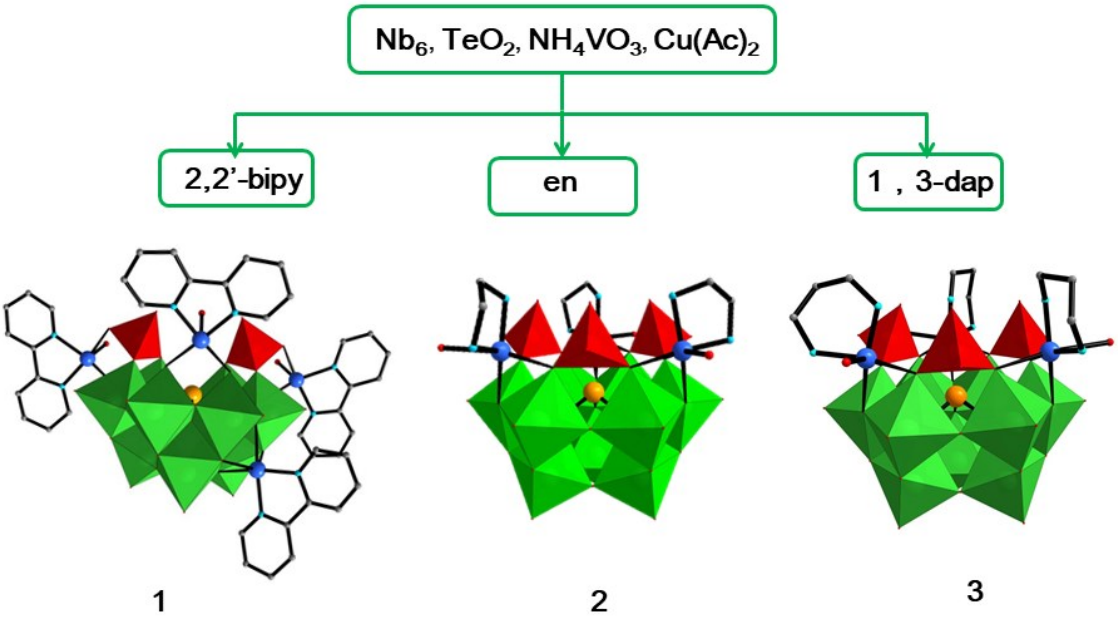

Figure S4 Combined ball-and-stick/polyhedral representation of the compounds **1-3**.

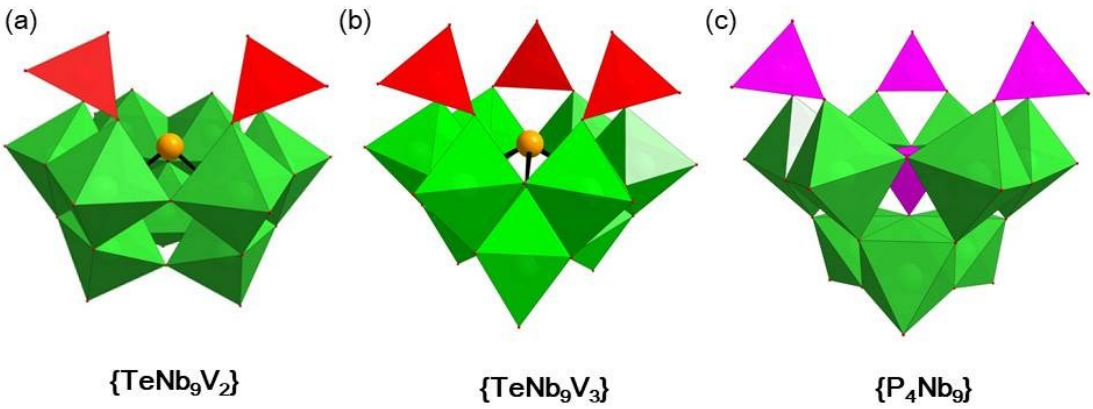

Figure S5 View of the structures of (a) $\{TeNb_9V_2\}$, (b) $\{TeNbV_3\}$ and (c) $\{P_4Nb_9\}$.

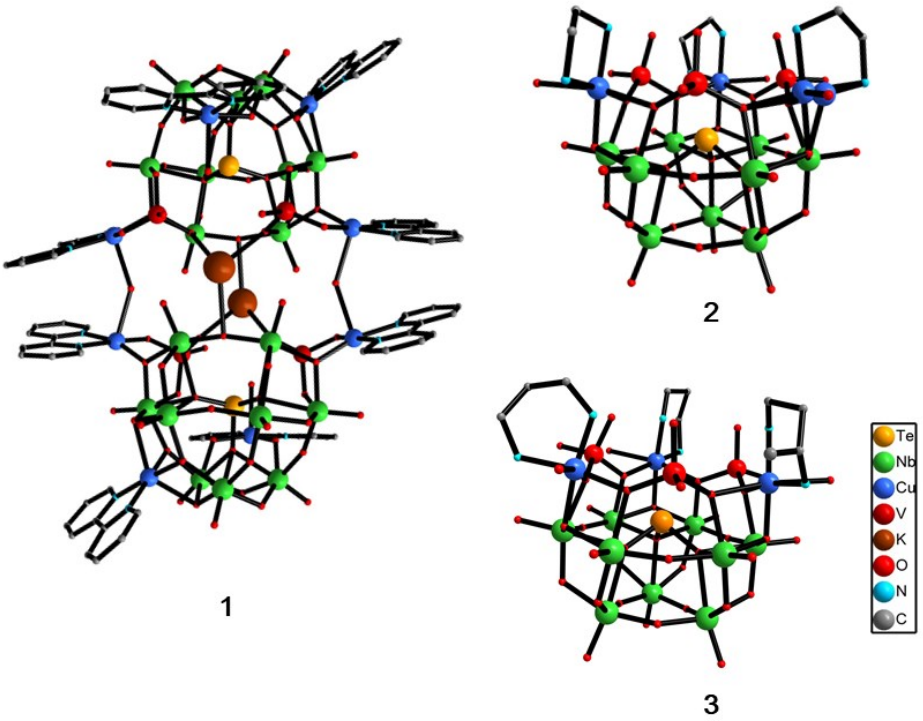

Figure S6 Ball-and-stick representation of the compounds **1**-**3**.

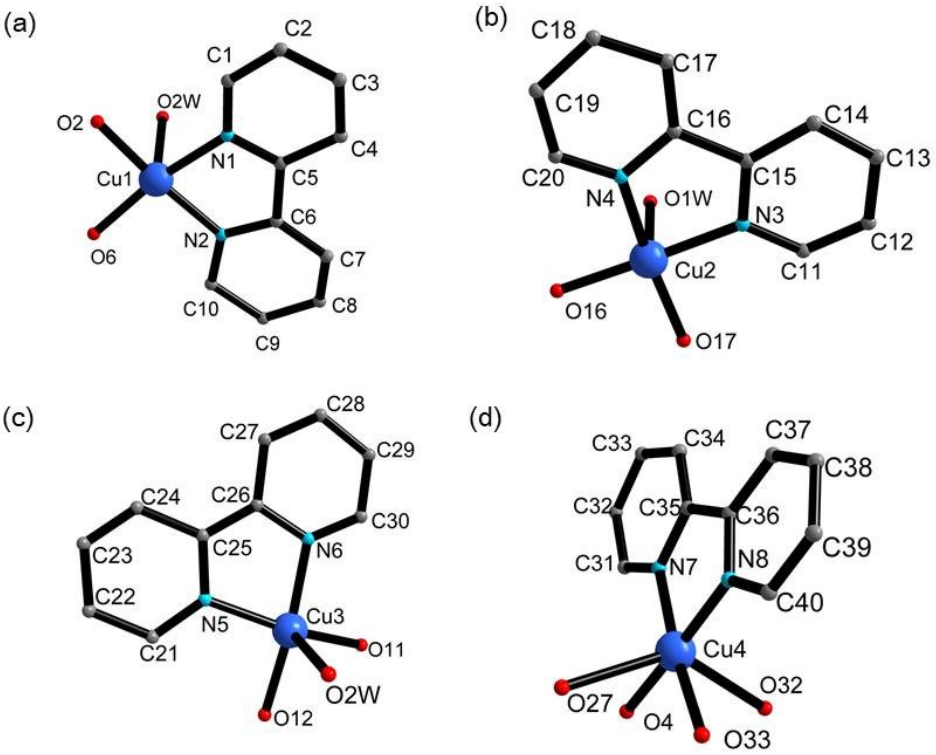

Figure S7 The coordination geometric frameworks of (a) Cu1, (b) Cu2, (c) Cu3, (d) Cu4 ions in compound **1.**

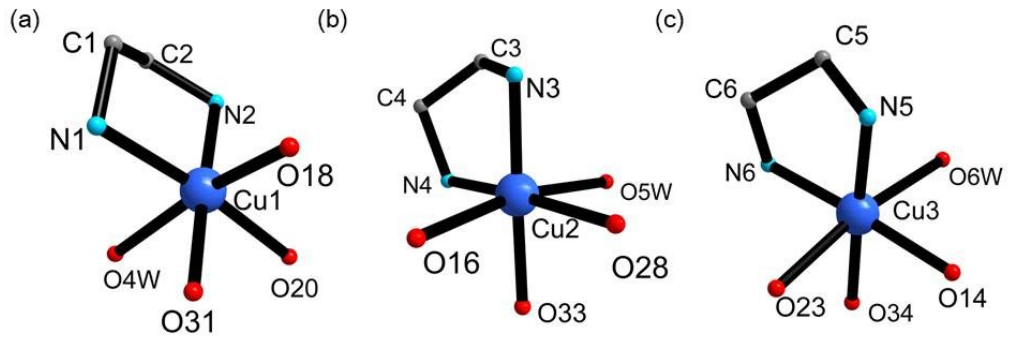

Figure S8 The coordination geometric frameworks of (a) Cu1, (b) Cu2, (c) Cu3 ions in compound **2.**

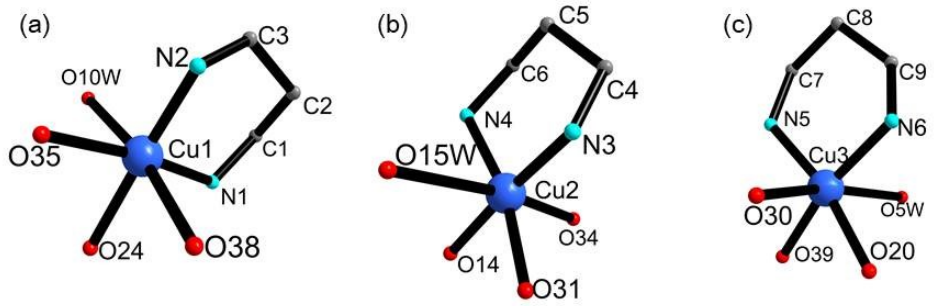

Figure S9 The coordination geometric frameworks of (a) Cu1, (b) Cu2, (c) Cu3 ions in compound **3.**

Table S7 Coordination bond length and bond angle of Cu atoms in compound **1** and some compounds with ligands 2,2'-bipy.

Compound	**Atom**	**Bond**	**Length/Å**	**Bond**	**Angle/°**
1	$\{Cu1N_2O_3\}$	Cu1–O	1.949(8)-2.404(8)	*cis* N/O–Cu–N/O	80.6(6)-102.5(3)
		Cu1–N	1.976(14)-2.008(11)	*trans* N/O–Cu–N/O	166.4(4)-172.4(5)
	$\{Cu2N_2O_3\}$	Cu2–O	1.945(8)-2.303(8)	*cis* N/O–Cu–N/O	81.9(4)-97.9(3)
		Cu2–N	1.978(10)-1.982(11)	*trans* N/O–Cu–N/O	169.1(4)-171.2(4)
	$\{Cu3N_2O_3\}$	Cu3–O	1.938(9)-2.384(8)	*cis* N/O–Cu–N/O	83.0(3)-101.5(4)
		Cu3–N	1.985(14)-2.016(14)	*trans* N/O–Cu–N/O	162.4(4)-173.9(5)
	$\{Cu4N_2O_4\}$	Cu4–O	1.992(8)-2.450(6)	*cis* N/O–Cu–N/O	73.4(7)-109.5(8)
		Cu4–N	1.987(11)-1.989(11)	*trans* N/O–Cu–N/O	136.1(0)-173.9(4)
$\{Nb_6O_{19}[Cu(2,2'\text{-bipy})]_2[Cu(2,2'\text{-bi-py})_2]_2\}$[S8]	$\{Cu1N_2O_3\}$	Cu1–O	1.963(3)-2.382(3)	*cis* N/O–Cu–N/O	75.92(12)-110.70(15)
		Cu1–N	1.974(4)-1.994(4)	*trans* N/O–Cu–N/O	173.37(15)-176.10(15)
$\{[Cu(2,2'\text{-bipy})][Cu(2,2'\text{-bipy})(H_2O)]Nb_6O_{19}\}$[S9]	$\{Cu1N_2O_3\}$	Cu1–O	1.965(3)-2.355(4)	*cis* N/O–Cu–N/O	77.31(12)-107.33(16)
		Cu1–N	1.994(5)	*trans* N/O–Cu–N/O	175.36(17)
	$\{Cu2N_2O_4\}$	Cu2–O	1.979(6)	*cis* N/O–Cu–N/O	75.72(12)-106.98(17)
		Cu2–N	1.967(3)-2.969(1)	*trans* N/O–Cu–N/O	163.17(32)-177.29(19)
	$\{Cu3N_4O_2\}$	Cu3–O	2.664(3)-2.736(3)	*cis* N/O–Cu–N/O	83.7(3)-96.2(2)
		Cu3–N	1.981(6)-2.019(6)	*trans* N/O–Cu–N/O	178.8(3)-179.4(3)
$\{Cu(2,2'\text{-bipy})\}_4\{Cu(2,2'\text{-bipy})(H_2O)\}_2(Nb_{16}O_{48})]\}$[S10]	$\{Cu1N_2O_3\}$	Cu1–O	1.934(5)-2.149(7)	*cis* N/O–Cu–N/O	80.56(6)-102.81(4)
		Cu1–N	2.00(33)-2.0376(4)	*trans* N/O–Cu–N/O	157.06(3)-167.06(9)
	$\{Cu3N_2O_3\}$	Cu3–O	1.896(2)-2.244(4)	*cis* N/O–Cu–N/O	81.80(2)-99.94(5)
		Cu3–N	1.989(6)-2.001(4)	*trans* N/O–Cu–N/O	164.07(6)-168.21(5)
$\{[Cu(H_2O)(2,2'\text{-bipy})]_2[CuNb_{11}O_{35}H_4]\}$[S11]	$\{Cu2N_2O_3\}$	Cu2–O	1.919(1)-2.329(5)	*cis* N/O–Cu–N/O	80.85(2)-99.50(9)
		Cu2–N	1.997(9)-1.999(4)	*trans* N/O–Cu–N/O	164.47(6)-173.44(9)
	$\{Cu3N_2O_3\}$	Cu2–O	1.906(1)-2.307(5)	*cis* N/O–Cu–N/O	80.80(4)-96.87(9)
		Cu2–N	1.99(57)-1.996(4)	*trans* N/O–Cu–N/O	163.89(0)-172.69(1)

Table S8 Coordination bond length and bond angle of Cu atoms in compound **2** and some compounds with ligands en.

Compound	**Atom**	**Bond**	**Length**	**Bond**	**Angle**
2	{$Cu1N_2O_4$}	Cu1–O	1.988(4)-2.574(8)	*cis* N/O–Cu–N/O	76.63(17)-96.7(9)
		Cu1–N	1.979(7)-2.022(6)	*trans* N/O–Cu–N/O	167.7(2)-170.3(0)
	{$Cu2N_2O_4$}	Cu2–O	1.971(5)-2.732(7)	*cis* N/O–Cu–N/O	78.07(17)-102.7(2)
		Cu2–N	1.983(7)-1.999(6)	*trans* N/O–Cu–N/O	166.6(2)-174.3(2)
	{$Cu3N_2O_4$}	Cu3–O	1.999(5)-2.701(8)	*cis* N/O–Cu–N/O	77.35(18)-101.6(5)
		Cu3–N	1.983(8)-2.017(6)	*trans* N/O–Cu–N/O	166.0(3)-168.0(2)
{$[Cu(en)_2][KNb_{24}O_{72}H_9]_2$}[S12]	{$Cu4N_4O_2$}	Cu4–O	2.737(2)-2.823(8)	*cis* N/O–Cu–N/O	84.80(4)-94.34(6)
		Cu4–N	1.963(3)-1.981(5)	*trans* N/O–Cu–N/O	178.31(8)-178.43(5)
	{$Cu10N_4O_2$}	Cu10–O	2.501(2)-2.876(6)	*cis* N/O–Cu–N/O	83.79(8)-96.56(3)
		Cu10–N	1.992(4)-2.013(1)	*trans* N/O–Cu–N/O	170.98(5)-179.40(5)
	{$Cu11N_4O_2$}	Cu11–O	2.491(8)-2.819(6)	*cis* N/O–Cu–N/O	83.74(8)-95.82(2)
		Cu11–N	1.989(9)-2.012(5)	*trans* N/O–Cu–N/O	171.58(6)-178.29(8)
{$[Cu(en)_2]_3[Cu(en)_2][H_2V_4Nb_6O_{30}]$}[S13]	{Cu1N4O2}	Cu1–O	2.372(1)	*cis* N/O–Cu–N/O	84.85(7)-95.14(3)
		Cu1–N	2.022(6)-2.023(4)	*trans* N/O–Cu–N/O	180.00(0)
	{$Cu2N_4O_2$}	Cu2–O	2.622(5)	*cis* N/O–Cu–N/O	84.50(4)-95.49(6)
		Cu2–N	2.008(0)-2.014(1)	*trans* N/O–Cu–N/O	180.00(0)
	{$Cu3N_4O_2$}	Cu3–O	2.690(4)	*cis* N/O–Cu–N/O	84.82(1)-95.17(9)
		Cu3–N	1.998(6)-2.016(6)	*trans* N/O–Cu–N/O	180.00(0)
	{$Cu4N_4O_2$}	Cu4–O	2.604(4)	*cis* N/O–Cu–N/O	84.80(2)-95.19(8)
		Cu4–N	1.984(7)-2.048(1)	*trans* N/O–Cu–N/O	180.00(0)
{$[Cu(en)(H_2O)]_2[HNb_6O_{19}]_2$}[S14]	{$Cu1N_2O_4$}	Cu1–O	1.965(9)-2.890(1)	*cis* N/O–Cu–N/O	75.98(2)-102.60(2)
		Cu1–N	1.951(2)-2.020(0)	*trans* N/O–Cu–N/O	174.58(3)-175.75(1)
	{$Cu2N_2O_4$}	Cu2–O	2.011(6)-2.890(1)	*cis* N/O–Cu–N/O	75.55(1)-115.89(9)
		Cu2–N	1.970(9)-2.006(02)	*trans* N/O–Cu–N/O	167.41(9)-175.54(4)

Table S9 Coordination bond length and bond angle of Cu atoms in compound **3** and some compounds with ligands 1,3-dap.

Compound	**Atom**	**Bond**	**Length/Å**	**Bond**	**Angle/°**
3	{$Cu1N_2O_4$}	Cu1–O	2.018(11)-2.603(18)	*cis* N/O–Cu–N/O	77.7(4)-99.5(9)
		Cu1–N	2.02(3)-2.08(2)	*trans* N/O–Cu–N/O	166.4(1)-173.3(7)
	{$Cu2N_2O_4$}	Cu2–O	1.991(12)-2.490(2)	*cis* N/O–Cu–N/O	77.8(5)-98.8(8)
		Cu2–N	1.95(3)-2.07(2)	*trans* N/O–Cu–N/O	166.7(6)-178.3(8)
	{$Cu3N_2O_4$}	Cu3–O	2.008(11)-2.617(3)	*cis* N/O–Cu–N/O	77.9(4)-100.7(8)
		Cu3–N	2.01(2)-2.11(2)	*trans* N/O–Cu–N/O	167.0(8)-176.7(7)
{[Cu(1,3-dap)$_2$]$_2$[Cu(1,3-dap)(H_2O)]$_2$[Ta_6O_{19}]}[S15]	{$Cu1N_2O_4$}	Cu1–O	1.986(8)-2.448(11)	*cis* N/O–Cu–N/O	76.14(4)-97.36(4)
		Cu1–N	2.031(12)-2.035(11)	*trans* N/O–Cu–N/O	165.10(9)-172.50(6)
[Cu(1,3-dap)$_2$(H_2O)$_2$][Cu(1,3-dap)$_2$-($B(OH)_3$)$_2$][$B_4O_5(OH)_4$]$_2$[S16]	{$Cu1N_4O_2$}	Cu1–O	2.530(1)	*cis* N/O–Cu–N/O	84.72(2)-95.27(8)
		Cu1–N	2.009(9)-2.024(4)	*trans* N/O–Cu–N/O	180.0(0)
	{$Cu2N_4O_2$}	Cu2–O	2.625(8)	*cis* N/O–Cu–N/O	86.08(2)-93.91(8)
		Cu2–N	2.030(9)-2.032(2)	*trans* N/O–Cu–N/O	180.0(0)
[Cu(1,3-dap)2]2[Cu(1,3-dap)]2H[*a*-$PW_{10.5}Cu_{1.5}O_{40}$][S17]	{$Cu1N_2O_4$}	Cu1–O	1.993(13)-2.721(1)	*cis* N/O–Cu–N/O	77.78(0)-95.41(7)
		Cu1–N	1.967(5)–1.980(0)	*trans* N/O–Cu–N/O	170.22(8)-172.23(6)
{[Cu(1,3-dap)$_2$(H_2O)][($H_6Nb_6O_{19}$)$_2$Cu(1,3-dap)$_2$]}[S18]	{$Cu1N_4O_2$}	Cu1–O	2.646(7)–2.696(3)	*cis* N/O–Cu–N/O	89.03(3)-92.31(8)
		Cu1–N	2.031(4)–2.038(4)	*trans* N/O–Cu–N/O	162.08(4)-173.48(3)

Section 3 Additional Measurements

The PXRD spectra of compounds **1-3** are in good agreement with the calculated spectra based on the results of single crystal X-ray diffraction, which prove that the samples used for testing are pure (Figure S10-S12). It is worth noting that the disappearance or intensity change of some peaks may be caused by the change of crystal orientation during grinding.

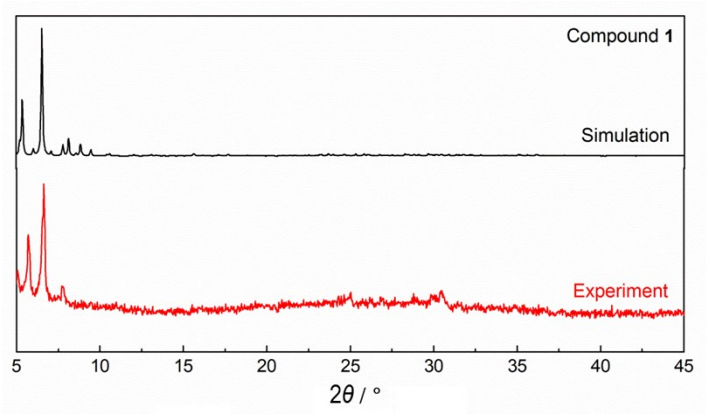

Figure S10 X-ray powder patterns of compound **1**.

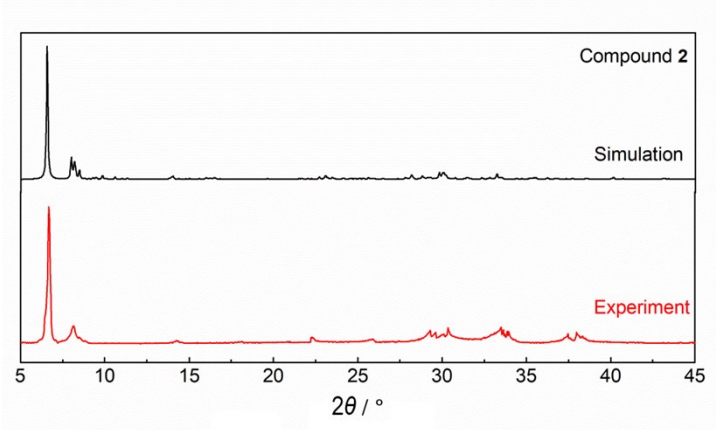

Figure S11 X-ray powder patterns of compound **2**.

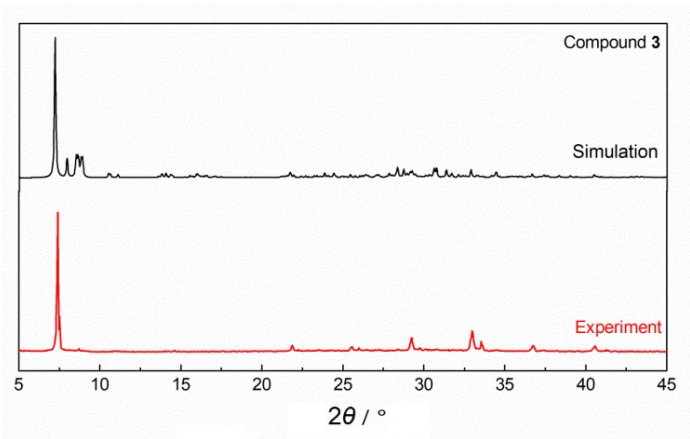

Figure S12 X-ray powder patterns of compound **3**.

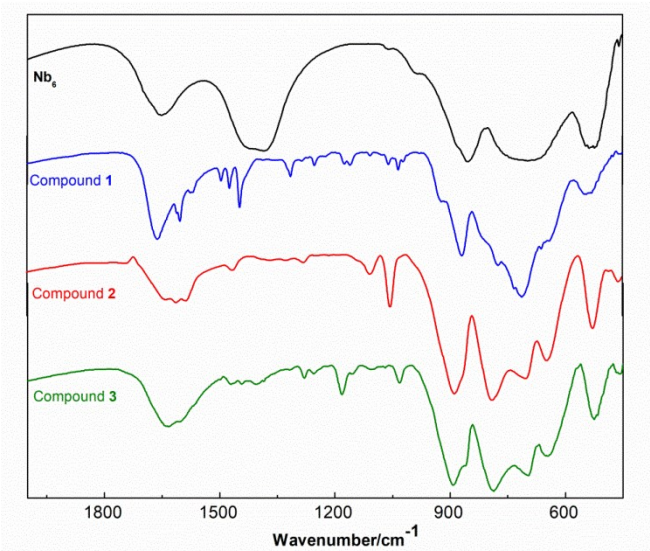

Figure S13 The IR spectra of **1**, **2**, **3** and $K_7H[Nb_6O_{19}]\cdot 13H_2O$.

The TG properties of **1-3** were measured under air atmosphere with a heating rate of 10 ℃ min^{-1} from 25 to 1100 ℃ (Figure S14-S16). The TG curves of **1** indicate two-step weight loss, while the weight loss of **2** and **3** can be regarded as one-step weight loss simply. For **1**, the first weight loss is 8.59 % in the range of 25-160 ℃, assigned to the release of 29 lattice water molecules (8.54% calculated). The second weight loss from 160 to 1000 °C is attributed to the loss of 2 coordination water, 2 guanidinium caions, 4 2,2'-bipy ligands and the partial sublimation of TeO_2 and V_2O_5. For **2,** the total weight loss is 20.94 % in the range of 25-800 ℃ corresponding to the removal of 10 lattice water molecules, 3 coordination water, 3 en ligands and the partial sublimation of TeO_2 and V_2O_5. For **3**, the TG curve gives a total loss of 11.77 % in the range of 25-1070 ℃ involving the loss of 11 lattice water molecules, 3 coordination water, 3 1,3-dap ligands and the partial sublimation of TeO_2 and V_2O_5.

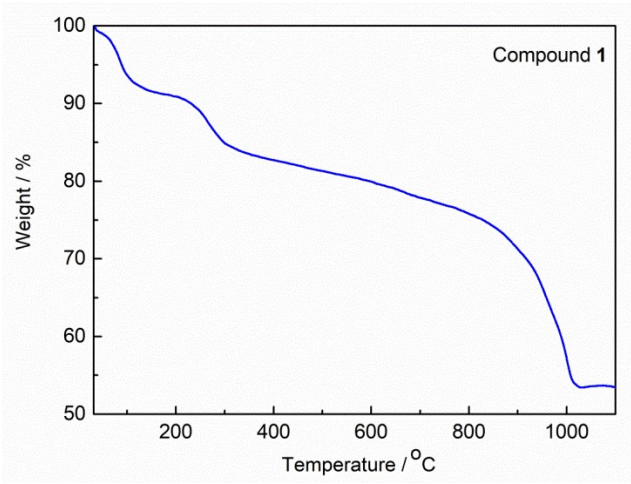

Figure S14 Thermogravimetric curve of **1**.

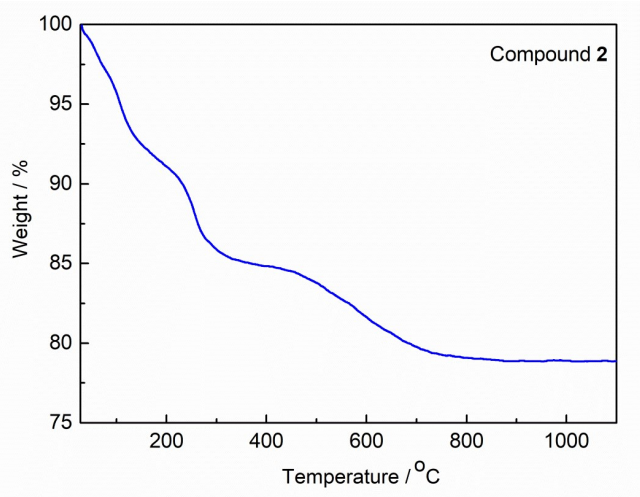

Figure S15 Thermogravimetric curve of **2**.

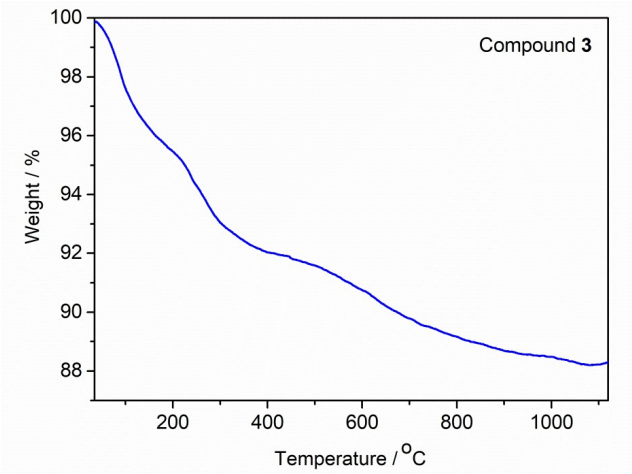

Figure S16 Thermogravimetric curve of **3**.

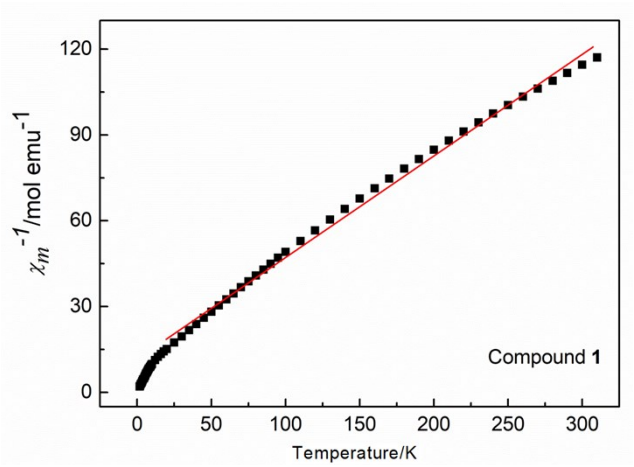

Figure S17 The temperature dependence of $1/\chi_m$ for **1**, and the red solid for **1** line represent the best-fit by the Curie-Weiss law.

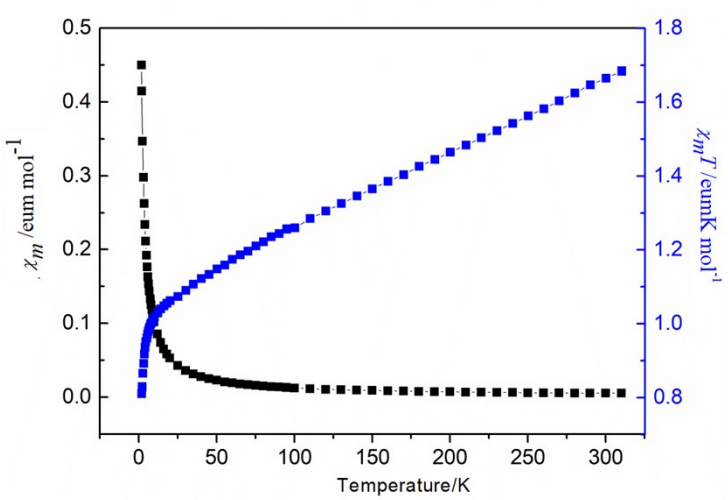

Figure S18 The plots of χ_m and $\chi_m T$ *versus* T for **2**.

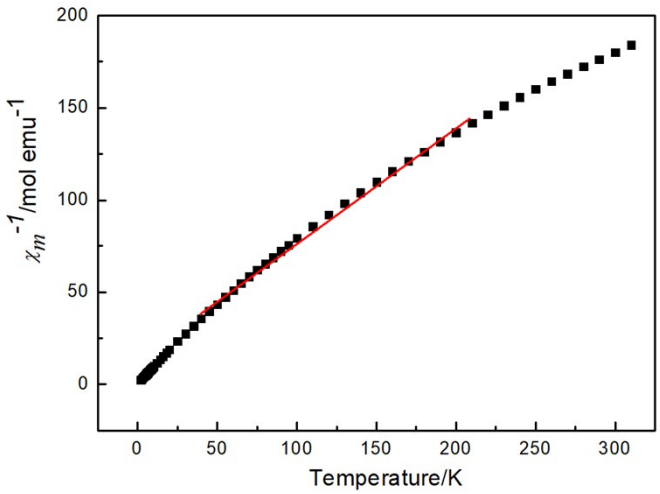

Figure S19 The temperature dependence of $1/\chi_m$ for **2**.

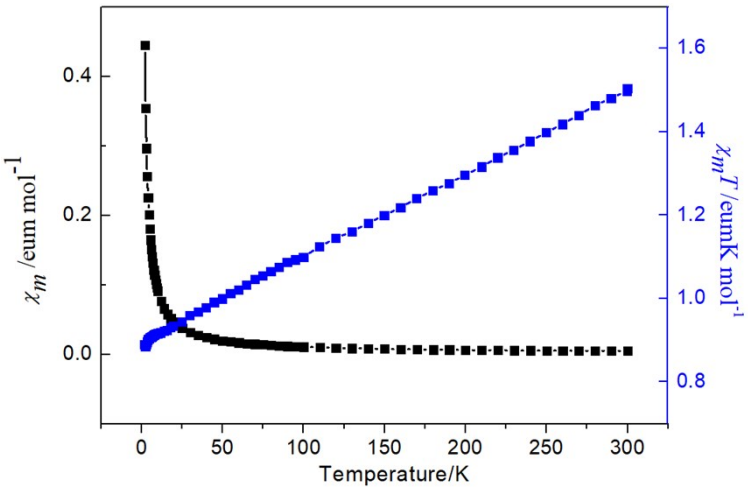

Figure S20 The plots of χ_m and $\chi_m T$ *versus* T for **3**.

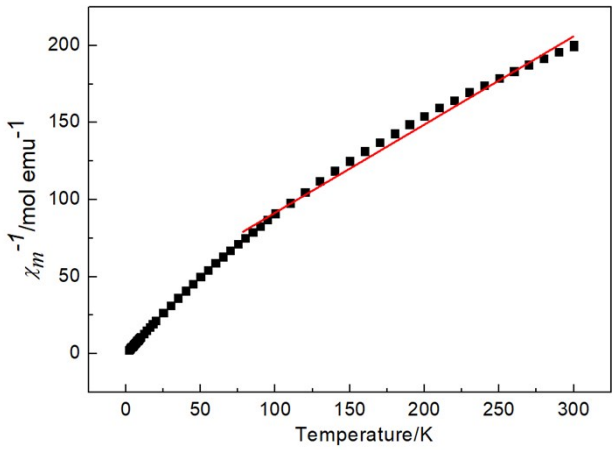

Figure S21 The temperature dependence of $1/\chi_m$ for **3**.

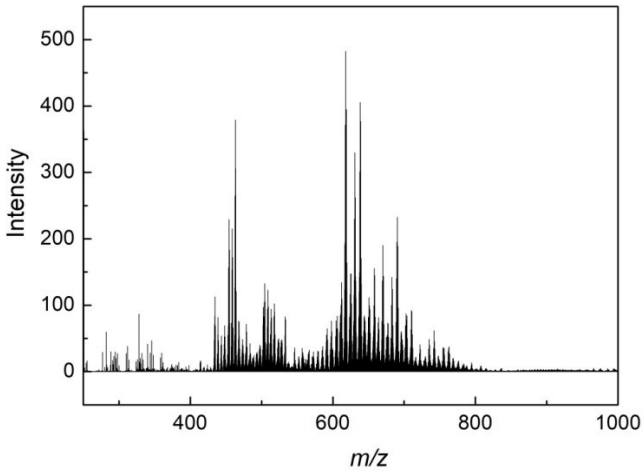

Figure S22 Negative-mode ESI-MS of compound **1** in aqueous solution.

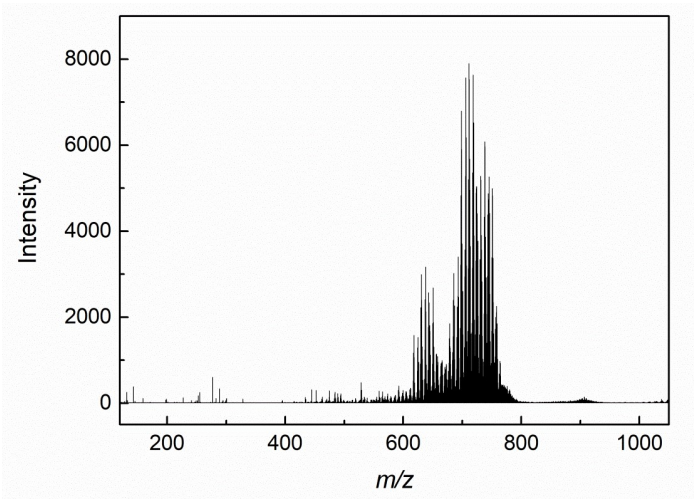

Figure S23 Negative-mode ESI-MS of compound **2** in aqueous solution.

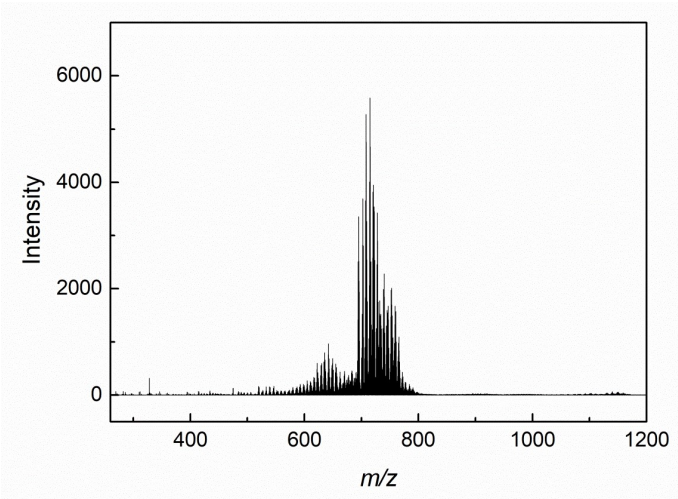

Figure S24 Negative-mode ESI-MS of compound **3** in aqueous solution.

Table S10 Assignment of mass spectral data for compound **1**.

Entry	Identification	Charge	Cal. m/z	Exp. m/z
1	$\{H_8K(CN_3H_6)_2(TeNb_9V_2O_{37})\}$	-4	456.23	456.28
2	$\{H_8(CN_3H_6)_3(TeNb_9V_2O_{37})\}$	-4	461.48	461.39
3	$\{H_8(CN_3H_6)_3(TeNb_9V_2O_{37})(H_2O)\}$	-4	465.98	465.94
4	$\{H_6K_2(CN_3H_6)[Cu(2,2'\text{-bipy})](TeNb_9V_2O_{37})\}$	-4	505.42	505.38
5	$\{H_6K_2(CN_3H_6)[Cu(2,2'\text{-bipy})](TeNb_9V_2O_{37})(H_2O)\}$	-4	509.92	508.88
6	$\{H_6K_2(CN_3H_6)[Cu(2,2'\text{-bipy})](TeNb_9V_2O_{37})(H_2O)_2\}$	-4	514.43	514.38
7	$\{H_6K_2(CN_3H_6)[Cu(2,2'\text{-bipy})](TeNb_9V_2O_{37})(H_2O)_3\}$	-4	518.93	518.78
8	$\{H_9K(CN_3H_6)_2(TeNb_9V_2O_{37})(H_2O)_2\}$	-3	620.66	620.69

9	$\{H_9K(CN_3H_6)_2(TeNb_9V_2O_{37})(H_2O)_3\}$	-3	626.66	626.58
10	$\{H_9K[Cu(2,2'\text{-bipy})](TeNb_9V_2O_{37})\}$	-3	641.83	641.75
11	$\{H_7K(CN_3H_6)_2[Cu(2,2'\text{-bipy})](TeNb_9V_2O_{37})(H_2O)_2\}$	-3	693.23	693.20

*The oxidation states of Cu, Te, V and Nb atoms in the formulas asigned to the peaks are +2, +4, +5 and +5, respectively.

Table S11 Assignment of mass spectral data for compound **2**.

Entry	Identification	Charge	Cal. m/z	Exp. m/z
1	$\{H_9[Cu(en)](TeNb_9V_3O_{39})(H_2O)\}$	-3	631.43	630.39
2	$\{H_8Na[Cu(en)](TeNb_9V_3O_{39})(H_2O)\}$	-3	637.76	637.85
3	$\{H_8Na[Cu(en)](TeNb_9V_3O_{39})(H_2O)_2\}$	-3	643.76	643.90
4	$\{H_7Na_2[Cu(en)](TeNb_9V_3O_{39})(H_2O)_2\}$	-3	651.09	651.00
5	$\{H_6Na[Cu(en)]_2(TeNb_9V_3O_{39})(H_2O)\}$	-3	678.30	678.33
6	$\{H_3Na_4[Cu(en)]_2(TeNb_9V_3O_{39})(H_2O)_2\}$	-3	706.29	706.24
7	$\{H_5[Cu(en)]_3(TeNb_9V_3O_{39})(H_2O)\}$	-3	711.52	711.47
8	$\{H_5[Cu(en)]_3(TeNb_9V_3O_{39})(H_2O)_2\}$	-3	717.52	717.48
9	$\{H_3NaK[Cu(en)]_3(TeNb_9V_3O_{39})(H_2O)\}$	-3	731.54	731.49
10	$\{H_2Na_2K[Cu(en)]_3(TeNb_9V_3O_{39})(H_2O)\}$	-3	738.87	738.86
11	$\{H_2Na_2K[Cu(en)]_3(TeNb_9V_3O_{39})(H_2O)_2\}$	-3	744.87	744.83

*The oxidation states of Cu, Te, V and Nb atoms in the formulas asigned to the peaks are +2, +4, +5 and +5, respectively.

Table S12 Assignment of mass spectral data for compound **3**.

Entry	Identification	Charge	Cal. m/z	Exp. m/z
1	$\{H_9[Cu(1,3\text{-dap})](TeNb_9V_3O_{39})\}$	-3	629.10	629.22
2	$\{H_8Na[Cu(1,3\text{-dap})](TeNb_9V_3O_{39})(H_2O)\}$	-3	642.43	642.50
3	$\{H_7Na_2[Cu(1,3\text{-dap})](TeNb_9V_3O_{39})(H_2O)\}$	-3	649.76	649.82
4	$\{H_5Na_2[Cu(1,3\text{-dap})]_2(TeNb_9V_3O_{39})(H_2O)\}$	-3	694.98	694.96
5	$\{H_4Na_3[Cu(1,3\text{-dap})]_2(TeNb_9V_3O_{39})\}$	-3	702.31	702.22
6	$\{H_4Na_3[Cu(1,3\text{-dap})]_2(TeNb_9V_3O_{39})\}(H_2O)_2\}$	-3	708.31	708.15
7	$\{H_3Na_4[Cu(1,3\text{-dap})]_2(TeNb_9V_3O_{39})\}(H_2O)_2\}$	-3	715.64	715.62

8	$\{H_3Na_4[Cu(1,3\text{-dap})]_2(TeNb_9V_3O_{39})\}(H_2O)_3\}$	-3	721.64	721.54
9	$\{H_3KNa_3[Cu(1,3\text{-dap})]_2(TeNb_9V_3O_{39})\}(H_2O)_3\}$	-3	727.01	727.11
10	$\{H_2KNa_2[Cu(1,3\text{-dap})]_3(TeNb_9V_3O_{39})\}(H_2O)_2\}$	-3	758.90	758.94

*The oxidation states of Cu, Te, V and Nb atoms in the formulas asigned to the peaks are +2, +4, +5 and +5, respectively.

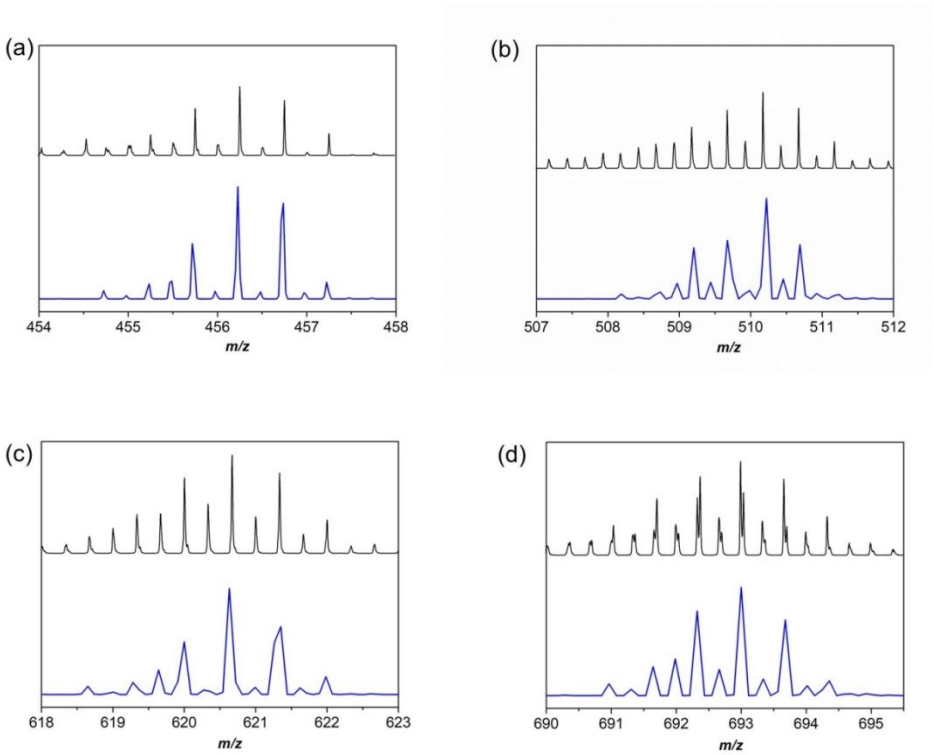

Figure S25 Selected experimental (black) and corresponding simulated (blue) negative-mode mass spectra of the isotopic envelopes (a) Entry 1; (b) Entry 5; (c) Entry 8; (d) Entry 11 for **1**.

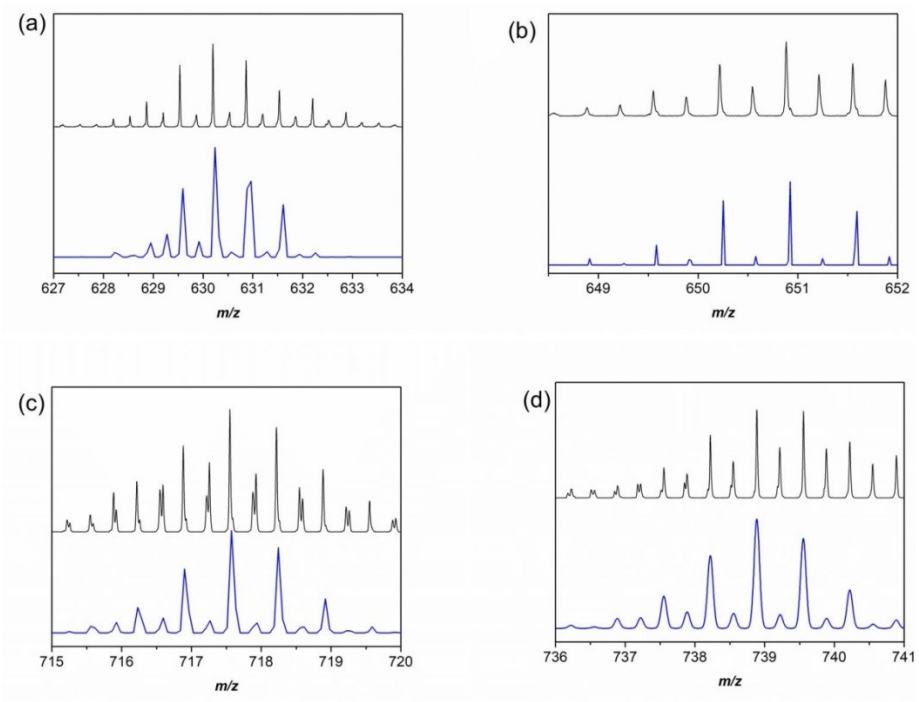

Figure S26 Selected experimental (black) and corresponding simulated (blue) negative-mode mass spectra of the isotopic envelopes (a) Entry 1; (b) Entry 4; (c) Entry 8; (d) Entry 10 for **2**.

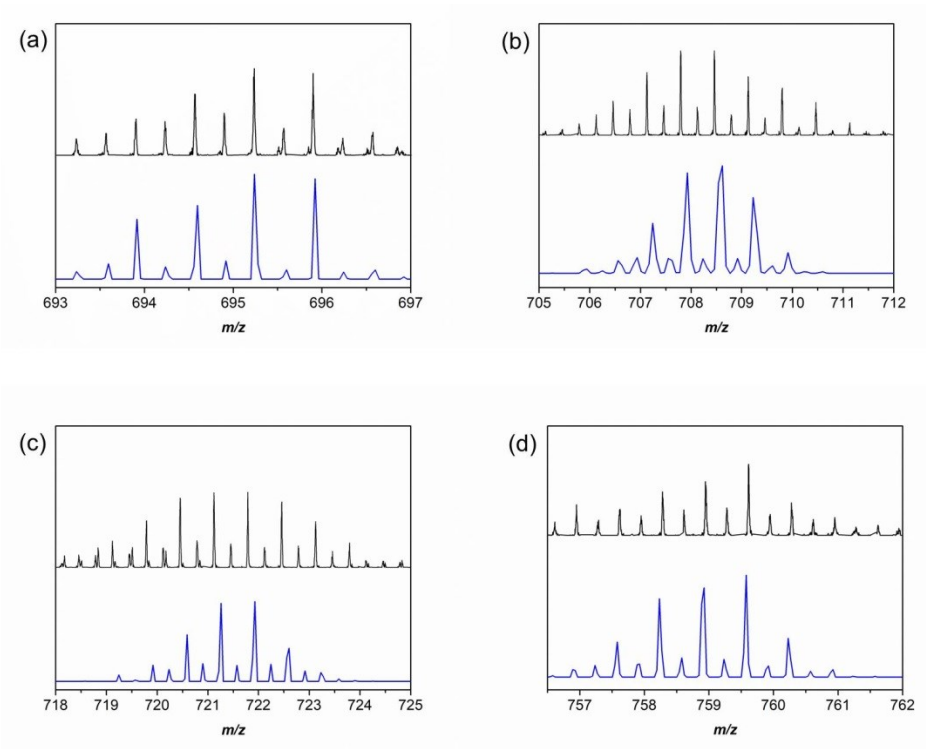

Figure S27 Selected experimental (black) and corresponding simulated (blue) negative-mode mass spectra of the isotopic envelopes (a) Entry 4; (b) Entry 6; (c) Entry 8; (d) Entry 10 for **3**.

Section 4 References

[S1] G. M. Sheldrick, *SADABS Bruker AXS Area Detector Scaling and Absorption*, version 2008/2001; University of Gottingen: Germany, 2008.

[S2] G. M. Sheldrick, Phase Annealing in *SHELX*-90: Direct Methods for Larger Structures, *Acta Crystallogr., Sect. A: Found. Crystallogr*. 1990, **46**, 467−473.

[S3] G. M. Sheldrick, A Short History of *SHELX*, *Acta Crystallogr., Sect. A: Found. Crystallogr.* 2008, **64**, 112−122.

[S4] I. D.Brown, D. Altermatt, Bond-valence parameters obtained from a systematic analysis of the inorganic crystal structure database, *Acta Crystallogr., Sect. B: Struct. Sci.* 1985, **41**, 244−247.

[S5] Q. Xu, B. Xu, H. Kong, P. He, J. Wang, T. Kannan, P. Ma, J. Wang and J. Niu, Synthesis and Characterization of a Crown-Shaped 36-Molybdate Cluster and Application in Catalyzing Knoevenagel Condensation, *Inorg. Chem*., 2020, **59**, 10665–10672.

[S6] D. Li, Q. Xu, Y. Li, Y. Qiu, P. Ma. J. Niu and J. Wang, A Stable Polyoxometalate-Based Metal–Organic Framework as Highly Efficient Heterogeneous Catalyst for Oxidation of Alcohols, *Inorg. Chem*., 2019, **58**, 4945–4953.

[S7] R. Wan, Z. Jing, Q. Xu, X. Ma, P. Ma, C. Zhang, J. Niu and J. Wang, Lacunary $\{S_{e4}V_{10}\}$ Heteropolyoxovanadate Precursor with Monometal, Metal-Richer-Sandwiched Derivatives $\{Se_8V_{20}M\}$ and $\{Se_8V_{20}M_3\}$: Correlations between the Synthesis, Structure, and Catalytic Property, *Inorg. Chem*., 2021, **60**, 2888–2892.

[S8] J. Wang, H. Niu and J. Niu, A novel Lindqvist type polyoxoniobate coordinated to four copper complex moieties: $\{Nb_6O_{19}[Cu(2,2'\text{-bipy})]_2[Cu(2,2'\text{-bipy})_2]_2\}\cdot 19H_2O$, *Inorg. Chem. Commun.,* 2008, **11**, 63−65.

[S9] J. Niu, X. Fu, J. Zhao, S. Li, P. Ma and J. Wang, Two-Dimensional Polyoxoniobates Constructed from Lindqvist-Type Hexaniobates Functionalized by Mixed Ligands, *Cryst. Growth Des.*, 2010, **10**, 3110–3119.

[S10] Z. Liang, Y. Qiao, M. Li, P. Ma, J. Niu and J. Wang, Two synthetic routes generate two isopolyoxoniobates based on $\{Nb_{16}\}$ and $\{Nb_{20}\}$, *Dalton Trans.,* 2019, **48**, 17709–17712.

[S11] J. Niu, G. Chen, J. Zhao, P. Ma, S. Li, J. Wang, M. Li, Y. Bai and B. Ji, Two Novel Copper–Undecaniobates Decorated by Copper–Organic Cations $[\{Cu(H_2O)L\}_2\{CuNb_{11}O_{35}H_4\}]_5$ (L=1,10-

phenanthroline, 2,2'-bipyridine) Consisting of Plenary and Monolacunary Lindqvist-Type Isopolyniobate Fragments, *Chem. Eur. J.*, 2010, **16**, 7082–7086.

[S12] Z. Wang, H. Tan, W Chen, Y. Li and E. Wang, A copper(II)–ethylenediamine modified polyoxoniobate with photocatalytic H_2 evolution activity under visible light irradiation, *Dalton Trans.*, 2012, **41**, 9882–9884.

[S13] G. Guo, Y. Xu, J. Cao and C. Hu, The $\{V_4Nb_6O_{30}\}$ Cluster: A New Type of Vanadoniobate Anion Structure, *Chem. Eur. J.,* 2012, **18**, 3493–3497.

[S14] R. P. Bontchev, E. L. Venturini and M. Nyman, Copper-Linked Hexaniobate Lindqvist Clusters-Variations on a Theme, *Inorg. Chem.*, 2007, **46**, 4483−4491.

[S15] G. Guo, Y. Xu, B. Chen, Z. Lin and C. Hu, Two novel polyoxotantalates formed by Lindqvist-type hexatantalate and Copper-amine complexes, *Inorg. Chem. Commun.,* 2011, 14, 1448−1451.

[S16] J. Wang and G. Yang, Novel borate supramolecular frameworks constructed from isolated B_4/B_5 clusters and 1-D B_{17}-based chains, *Inorg. Chem. Commun.,* 2017, 85, 92−95.

[S17] H. Chen, Q. Wu, J. Zhao, S. Li, J. Wang and J. Niu, Polyoxotungstate clusters: syntheses, characterization, and crystal structures of $[Cu^{II}(1,3\text{-dap})_2]_2[Cu^{II}(1,3\text{-dap})]_2H[\alpha\text{-}PW_{10.5}O_{40}]$ and $[Cu^{I}(phen)_2]_3[\alpha\text{-}PW_{12}O_{40}]$, *J. Coord. Chem.*, 2010, **63**, 1463–1472.

[S18] G. Wang, P. Ma, F. Li and J. Wang, A polyoxoniobate constructed from Lindqvist-type hexaniobates and copper coordinated cations, *J. Coord. Chem.*, 2011, **64**, 2718–2726.